Chapter 5

Formation of periodic magnetic field structures in overdense plasmas

The role played by the angle of incidence of a short pulse laser in the generation of magnetic field via. Weibel instability from overdense plasmas is investigated with the help of three dimensional (3D) particle-in-cell (PIC) simulations. The simulations have been done for different cases by varying the angle of incidence. The laser pulse gets self-focussed at a short distance in case of normal incidence which causes a rise in the axial intensity up to several times the fundamental laser intensity. Strong current filamentation leading towards the generation of high magnetic fields across the current filament is observed. In case of oblique incidence, vacuum heating becomes effective which causes the emission of energetic electron jets in a periodic pattern resulting in the formation of periodic density ripple like structures at the plasma front surface. These periodic structures carry forward and return currents leading towards the generation of periodic magnetic field structures having strong magnetic fields. The periodic structures are observed to have inter spacing distance same as that of the incident laser wavelength. The magnetic energy is observed to be highest in case of normal incidence due to strong current filamentation. Changing the angle of incidence to oblique weakens the filamentation which causes a reduction in the magnetic energy.

5.1 Background of the study

Generation of high amplitude magnetic fields has been an interesting and important area of research since many years in the field of laser plasma interactions [1–3]. Weibel instability [4] is mostly responsible for the generation of quasi-static magnetic-fields. The other possible sources of magnetic field generation are the non-parallel temperature and density gradients [i.e., $\partial B/\partial t = (1/n_e e)(\nabla T_e \times \nabla n_e)$] [5, 6] and the laser ponderomotive force [7]. Due to Weibel instability, the forward and return currents get separated which causes the generation of quasi-static ordered magnetic field configurations. This is followed by the tearing and coalescence instabilities, which produce current channels and hence filamentary magnetic field structures [3]. Pukhov and Meyer-ter Vehn [8] and Lasinski et al. [9] with the help of two dimensional (2D) particle-in-cell (PIC) simulations have shown that Weibel instability causes the break up of fast electrons into current filaments. Okada et al. [10] has also observed this filamentation in the fast ignitor (FI) scheme with the help of three dimensional (3D)-PIC simulations. Sentoku et al. [11] has observed the generation of layered current sheets which at later times partially merge with each other to form isolated magnetic channels in their 3D-PIC simulations. It was found that the fast electron energy flow was distributed inside as well as outside the magnetic channels.

It is well known that large quasi-static magnetic fields are generated via the mechanisms discussed above when the laser is incident normally on the target but an obliquely incident laser has a considerable effect on the magnetic field generation. In sharply-edged overdense plasmas, laser absorption can occur in an optical skin depth by both collisional and collision less processes such as inverse bremsstrahlung [12], $\vec{J}\times\vec{B}$ heating [13], vacuum heating [14], and anomalous skin-layer heating [15]. Tatarakis et al. [16] and Mondal et al. [3] have reported the generation of huge magnetic fields when a highly intense short pulse laser is incident obliquely on the plasma surface. Sentoku et al. [17] in their 2D-PIC simulations have demonstrated the formation of high energetic electron jets and the generation of megagauss magnetic fields in the coronal plasma for both s- and p-polarized lasers under oblique incidence. The magnetic fields generated due to Weibel instability are small and weak at the linear stage and hence do not have a remarkable effect on the high energy electron transport. However, when the magnetic fields get nonlinearly saturated, they impact more on

the high energy electron flow. Thus, it is very important to study the saturation of the generated magnetic fields. Okada and Ogawa [18] have investigated the nonlinear saturation of self-generated magnetic fields of Weibel instabilites and have found that the saturation is determined by the laser intensity and the plasma density.

In the present work, we investigate the role of the angle of incidence of a short pulse laser on magnetic field generation in overdense plasmas with the help of 3D-PIC simulations using the code Picpsi-3D [19]. The simulations have been done for three different angles of incidence. The formation of current filaments as well as filamentary magnetic field structures have been observed. The formation of current filaments is found to be much stronger when the laser is incident normally on the target. When the laser is incident obliquely, the formation of periodic density ripple like structures are observed which become more prominent for higher angles of incidence. These periodic structures carry forward and return currents, which produce periodic magnetic field patterns across the density ripples. 2D-PIC simulations to investigate the laser-plasma interactions when the laser is incident obliquely on the plasma target dominate the existing literature. 3D-PIC simulations provide a better insight of the processes occurring in these interactions specially on the target surface. To our knowledge, no 3D-PIC simulations have been done to study the phenomena which occur when the laser is incident obliquely on the target.

5.2 3D-PIC Simulation Model

The simulations have been done with a linearly polarized laser pulse (polarized in the Y direction) of wavelength $\lambda = 1$ μm, normalized electric field amplitude $a_0 (= eE_0/m_e\omega c) \approx 6$ which corresponds to an intensity of 5×10^{19} W/cm^2, pulse duration 50 fs (FWHM) incident on an overdense plasma target of density 3.5×10^{21} cm^{-3} (3.14 n_c). Here, $n_c = m_e\omega^2/4\pi e^2$ is the critical density where e and m_e are the charge and mass of an electron respectively, ω is the laser frequency, E_0 is the laser electric field amplitude and c is the speed of light. The electron plasma frequency is given as $\omega_{pe} = \sqrt{4\pi n_e e^2/m_e}$ where n_e is the electron plasma density. The spot size of the laser pulse is 3 μm (FWHM) and the laser period T_0 is 3.3 fs. The simulations have been done for three different cases. In the first case, the laser is incident normally

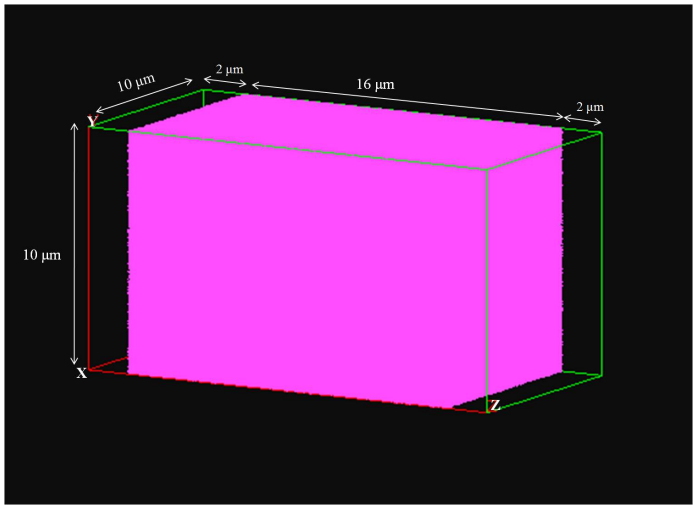

Fig. 5.1: 3D-PIC geometry of the simulation box when the laser is incident normally ($\theta = 0^0$) on the target.

($\theta = 0^0$) on the target along Z direction. A simulation box of dimensions 10 μm $\times$ 10 μm $\times$ 20 μm consisting of $100 \times 100 \times 200$ cells has been used. The overdense plasma slab is sharply edged and is located at a distance of 2 μm from the left boundary of the simulation box as shown in Fig. 5.1. In the second case, the laser is incident

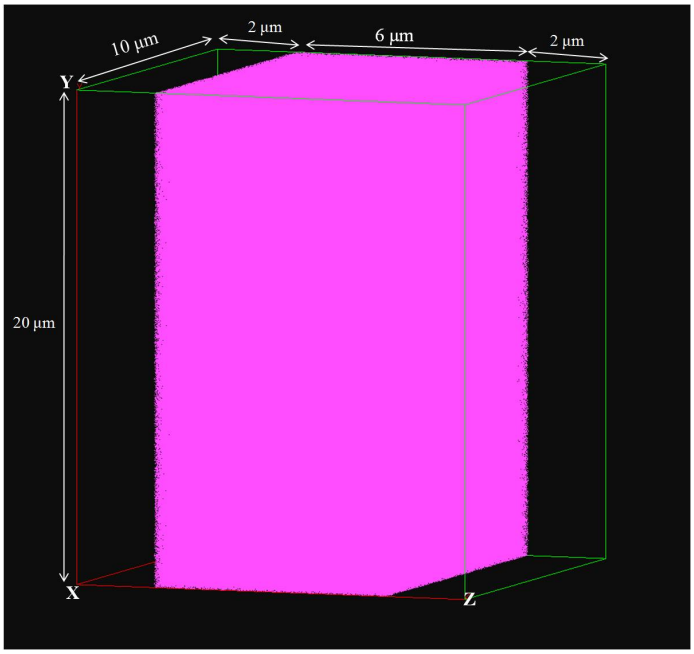

Fig. 5.2: 3D-PIC geometry of the simulation box when the laser is incident obliquely ($\theta = 30^0, 60^0$) on the target.

obliquely at $\theta = 30^0$ on the target. In the third case, the incident angle is changed to $\theta = 60^0$. In the last two cases, a simulation box of dimensions 10 μm $\times$ 20 μm $\times$ 10 μm consisting of $100 \times 200 \times 100$ cells has been used as shown in Fig. 5.2 and YZ is

the plane of incidence. Absorbing boundary conditions have been incorporated along all the three dimensions. The simulations are done with 25 macroparticles per cell. The ions considered in this simulation are protons with mass $m_i = 1836\ m_e$ and $Z = 1$. The plasma is initially assumed to be cold with $T_e = T_i = 0$, where T_e and T_i are electron and ion temperatures respectively.

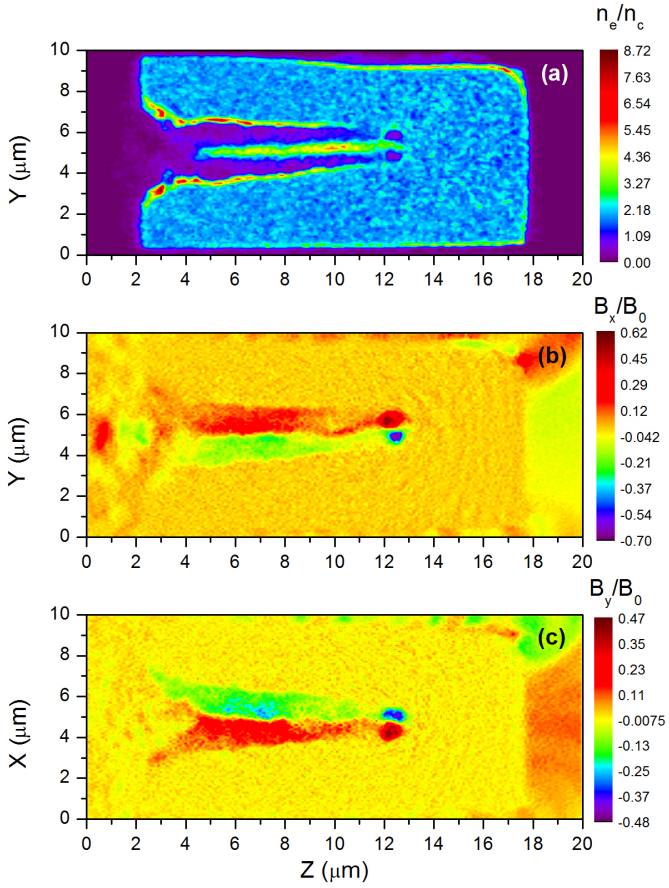

Fig. 5.3: (a) Electron density distribution in the central YZ plane (X = 5 μm). Magnetic field generated along (b) X direction B_x in the central YZ plane (X = 5 μm), (c) Y direction B_y in the central XZ plane (Y = 5 μm) at time 107.72 T_0 for $\theta = 0^0$. The electron density n_e is normalized by the critical density $n_c = 1.12 \times 10^{21}$ cm^{-3}. The magnetic field B_x is normalized by the laser magnetic field B_0.

5.3 Results and Discussion

In the first case, when the laser is incident normally ($\theta = 0^0$) on the target, a strong current carrying filament is formed which can be observed clearly from Fig. 5.3 (a) which represents the electron density distribution at time 107.72 T_0. The formation

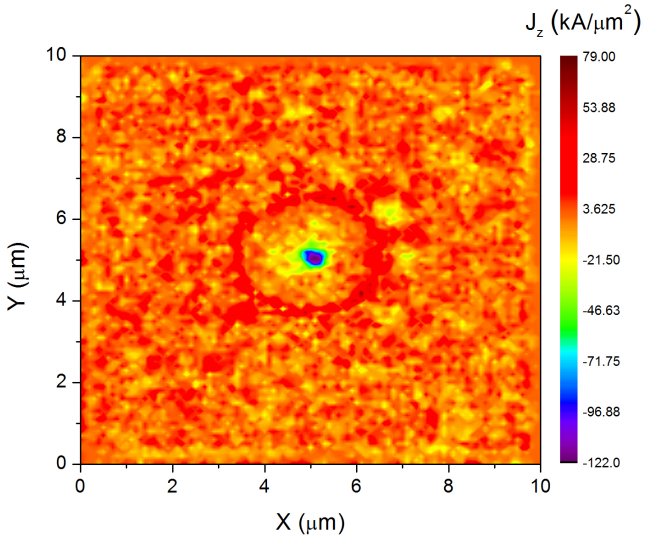

Fig. 5.4: Current density distribution along Z direction J_z (kA/μm^2) in the XY plane (Z = 6 μm) at time 107.72 T_0 for $\theta = 0^0$.

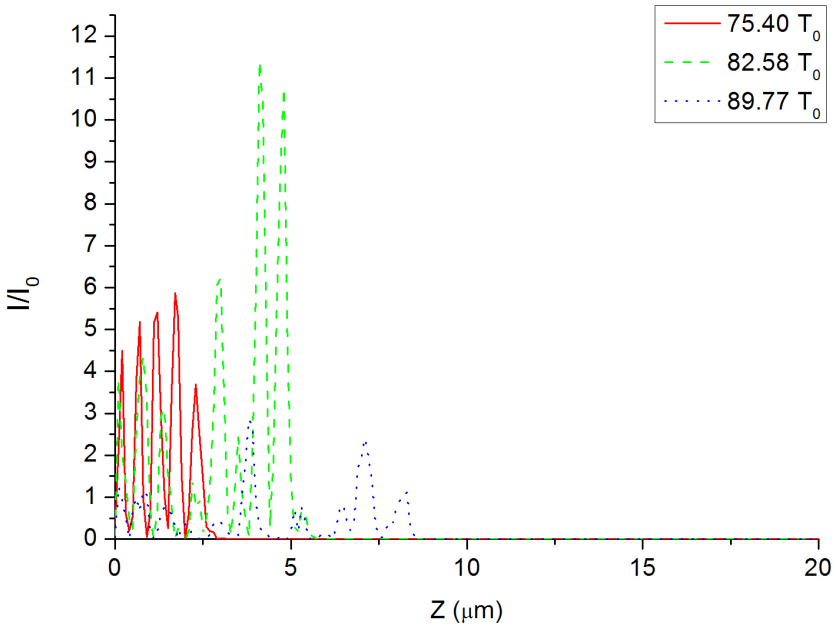

Fig. 5.5: Axial intensity I vs Z (μm) for $\theta = 0^0$ at times 75.40 T_0 (red solid), 82.58 T_0 (green dashed) and 89.77 T_0 (blue dotted). The intensity is normalized by the fundamental laser intensity I_0.

of magnetic channels across this current carrying filament is observed in Fig. 5.3 (b) and 5.3 (c) which displays the magnetic field generated along X and Y directions. A large magnetic field of the order of $\approx$ 400 MG is generated along X and that of the order of $\approx$ 200 MG is generated along Y direction. The current filament formed at the center of the XY plane carrying current in the forward direction and the return

cold currents are shown in Fig. 5.4. Tatarakis et al. [16] have reported the generation of magnetic fields of peak amplitudes greater than 340 MG and below 460 MG during the interaction of a short pulse (0.7-1 ps) ultrahigh intensity ($> 10^{19}$ W cm^{-2}) laser-solid target interaction. The laser intensity and the amplitudes of mag-

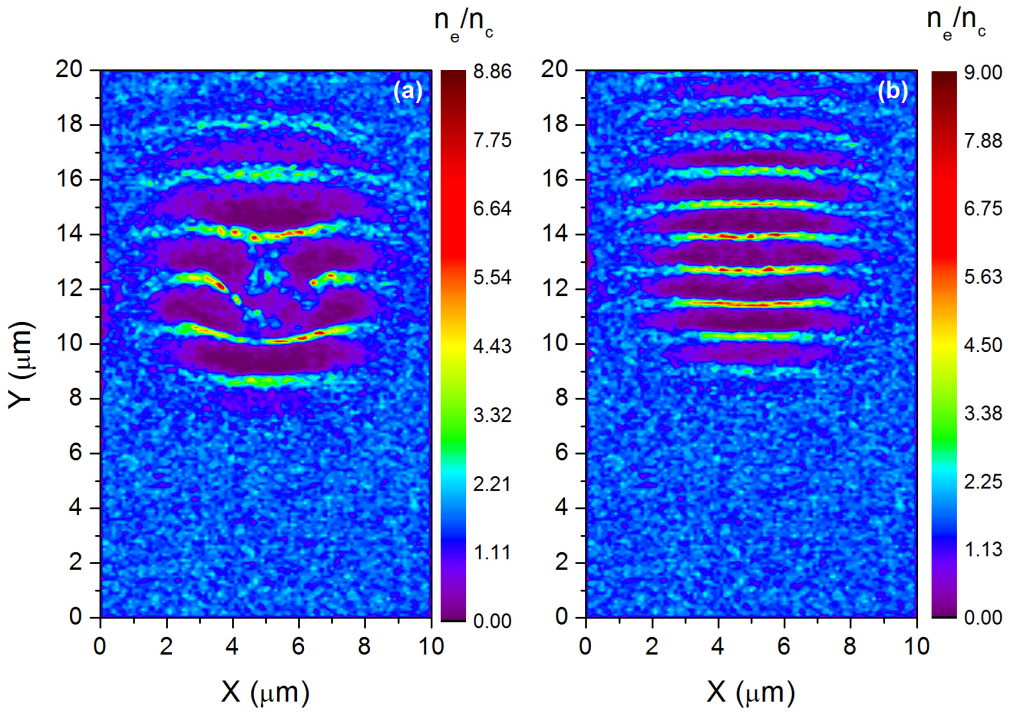

Fig. 5.6: Electron density distribution in the XY plane at the plasma surface (Z = 2 μm) for (a) $\theta = 30^0$ and (b) $\theta = 60^0$ at time 75.40 T_0. The electron density n_e is normalized by the critical density $n_c = 1.12 \times 10^{21}$ cm^{-3}.

netic fields generated in our simulations are quite analogous with their experimental observations. The magnetic channels which are formed spread over a region of a few micrometers in the plasma which is similar to the magnetic channel structural scale length as observed by Sentoku et al. [11] in their 3D-PIC simulations. Since, we have $n_e < \gamma n_c$ where $\gamma = \sqrt{1 + a_0^2/2}$ is the relativistic Lorentz factor, the laser pulse may penetrate into the overdense plasma slab due to relativistically induced transparency effects [20–22]. As the laser pulse penetrates the overdense plasma, it gets focused at a very short distance of ≈ 2 μm and the axial intensity of the laser rises up to ≈ 11 times the fundamental laser intensity. Beyond this length, the central current filament causes the filamentation of the laser pulse and the intensity decreases on further penetration into the plasma as shown in Fig. 5.5. Such kind of laser pulse focusing and formation of micron sized magnetic channels were also observed in 3D-PIC simulations reported by Naumova et al. [23] in case of underdense but

near-critical plasma. However, in our case, we have observed stronger filamentation of the laser pulse for a bit higher timescale as the plasma is overdense.

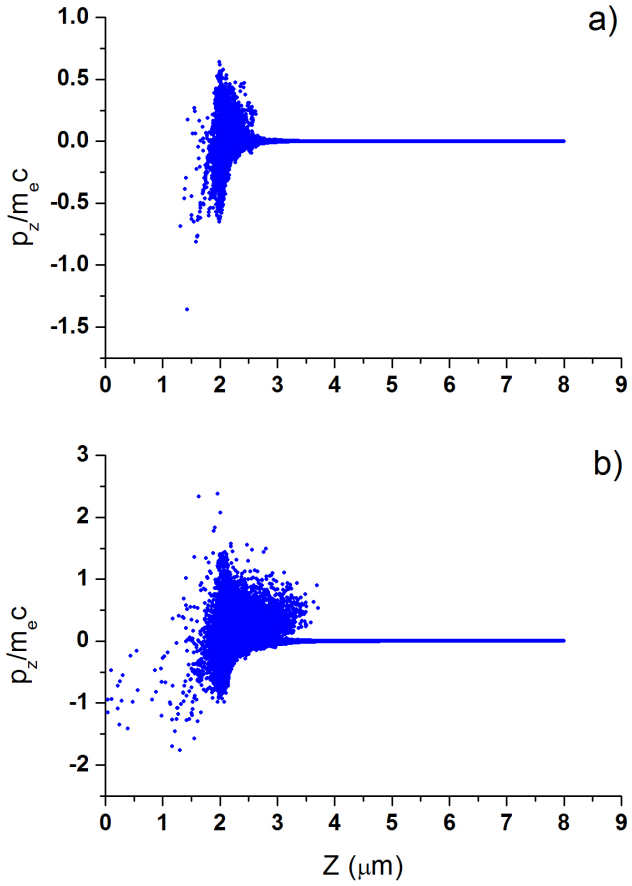

Fig. 5.7: Electron phase space p_z/m_ec vs Z(μm) for $\theta = 60^0$ at time (a) 64.63 T_0 and (b) 68.22 T_0.

In the second and third cases, where the laser pulse is incident obliquely on the target, the formation of density channels can be clearly observed in Fig. 5.6 (a) and (b) which depicts the electron density distribution at the plasma surface (Z = 2μm) at time 75.40 T_0 at $\theta = 30^0$ and $\theta = 60^0$ respectively. These density ripple like structures are formed due to vacuum heating. Since we have used a p-polarized laser, it is much favourable for vacuum heating. The laser electric field drags the electrons out of the plasma surface and as the electric field reverses its direction at later times, the electrons go back into the plasma again which results in an efficient heating of electrons. Fig. 5.7 shows the electron momentum phase space (p_z/m_ec vs Z) for $\theta = 60^0$ at different times. The laser electric field drags the electrons out of the plasma surface at time 64.63 T_0 as shown in Fig. 5.7 (a). The electrons gain more

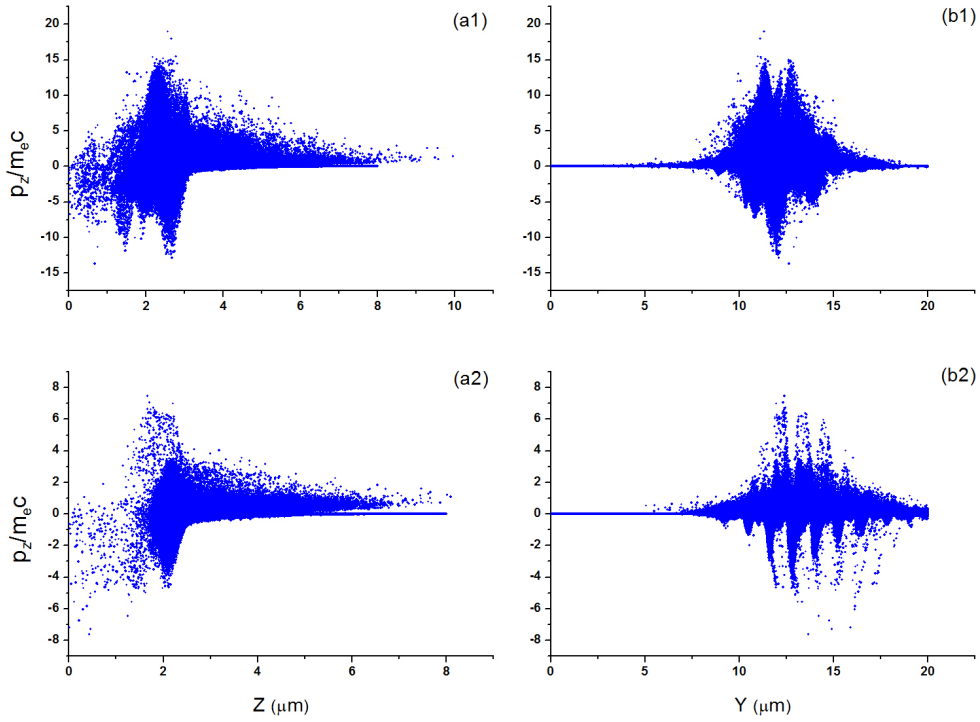

Fig. 5.8: Electron phase space p_z/m_ec vs Z (μm) for (a1) $\theta = 30^0$, (a2) $\theta = 60^0$ and electron phase space p_z/m_ec vs Y (μm) for (b1) $\theta = 30^0$, (b2) $\theta = 60^0$ at time 75.40 T_0.

momentum in the vacuum at a later time 68.22 T_0 as shown in Fig. 5.7 (b). Thus, the electrons at the plasma surface start gaining energy due to vacuum heating. Fig. 5.8 (a1) and (a2) represents the electron momentum phase space (p_z/m_ec vs Z (μm)) at $\theta = 30^0$ and 60^0 respectively at time 75.40 T_0. It can be observed that electrons are dragged out of the plasma surface at Z = 2μm and sent back with almost equal momenta. Vacuum heating would be more effective for higher angle of incidences as the laser electric field component normal to the plasma surface becomes stronger with the increase in angle of incidence. Hence, the density ripples are observed to be much more prominent for $\theta = 60^0$ as compared to that for $\theta = 30^0$. However, at $\theta = 30^0$, electrons gain more momentum as the laser is absorbed more efficiently due to $\vec{J} \times \vec{B}$ absorption. The inter spacing distance between these density ripples is almost equal to the laser wavelength ($\lambda = 1$ μm) in case of $\theta = 60^0$. At $\theta = 30^0$, the periodicity in the structures start getting deteriorated as $\vec{J} \times \vec{B}$ force starts dominating the electron heating process on reducing the angle of incidence. These periodic structures or density ripples carry forward and return currents which are

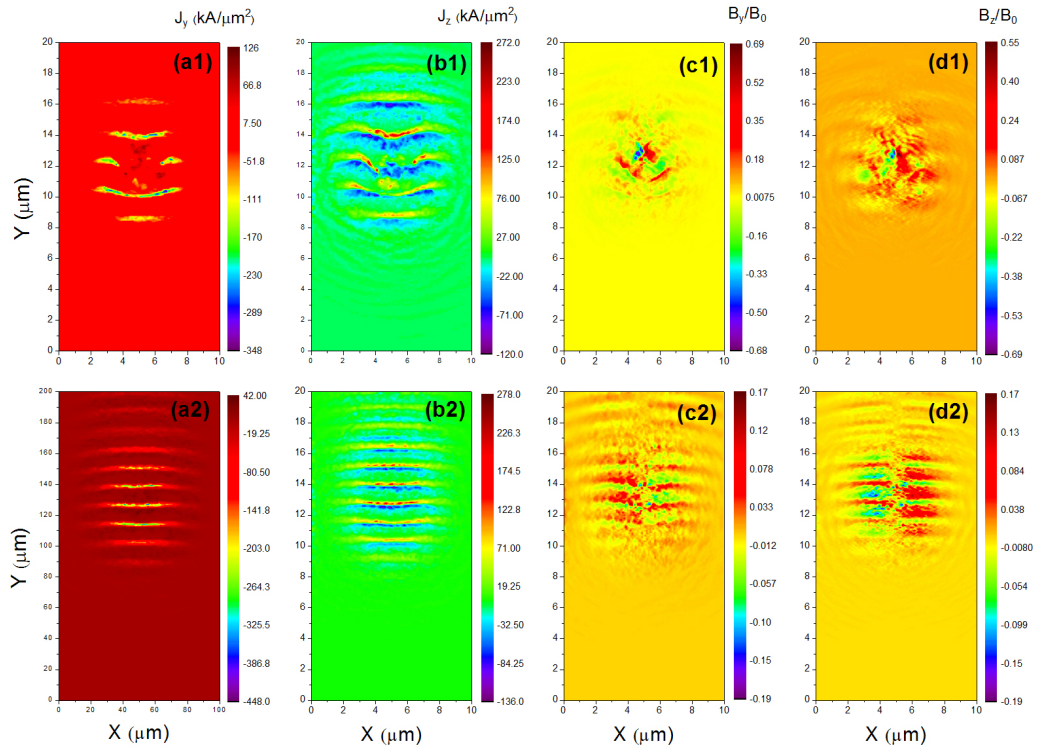

Fig. 5.9: Current density along (a1 and a2) Y direction J_y (kA/μm^2), (b1 and b2) Z direction J_z (kA/μm^2) for $\theta = 30^0$ and 60^0 respectively and magnetic field along (c1 and c2) Y direction B_y, (d1 and d2) Z direction B_z for $\theta = 30^0$ and 60^0 respectively at time 75.40 T_0 at the plasma surface (Z = 2 μm) in the XY plane. The magnetic field B_y and B_z are normalized by the laser magnetic field B_0.

responsible for the formation of magnetic channels across these ripples. The current density and magnetic fields generated across these ripples along Y and Z directions are plotted in Fig. 5.9. Magnetic fields of the order of $\approx$ 400 MG and $\approx$ 100 MG are generated across these ripples at $\theta = 30^0$ and 60^0 respectively. Fig. 5.8 (b1) and (b2) represents the electron momentum phase space (p_z/m_ec vs Y (μm)) at $\theta = 30^0$ and 60^0 respectively at time 75.40 T_0. It can be observed that electron jets are emitted from the plasma surface more prominently in a periodic pattern at $\theta = 60^0$. This periodic emission of electron jets causes the formation of density ripples. Sentoku et al. [17] have shown that high energetic electron jets are emitted when the laser is obliquely incident on the target and multi megagauss magnetic fields are generated around these electron jets. These magnetic fields are generated in the coronal underdense plasma which is put in front of the critical surface. However, in our case we have a sharply edged boundary between vacuum and the overdense plasma. Here, though

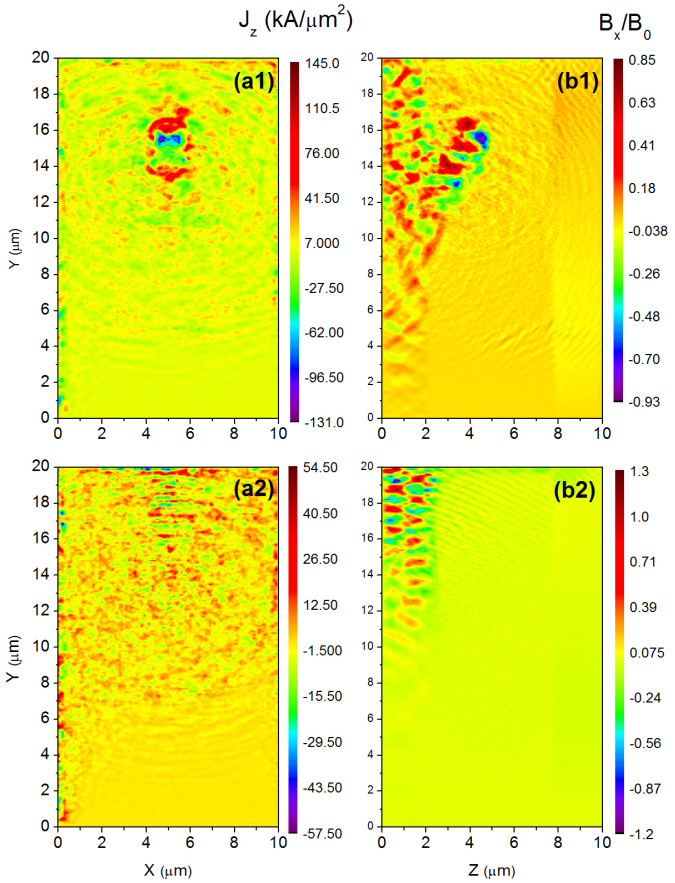

Fig. 5.10: Current density along (a1 and a2) Z direction J_z (kA/μm^2) in the XY plane at Z = 4 μm for $\theta = 30^0$ and 60^0 respectively and magnetic field along (b1 and b2) X direction B_x in the central YZ plane (X = 5 μm) for $\theta = 30^0$ and 60^0 respectively at time 89.77 T_0. The magnetic field B_x is normalized by the laser magnetic field B_0.

we have considered the overdense plasma target of low density (3.14 n_c), such kind of density ripples can also be observed for relatively high density targets on using a laser pulse of higher intensity. When the laser is incident at an angle $\theta = 30^0$, the laser penetrates up to some distance inside the plasma due to strong $\vec{J} \times \vec{B}$ force and a part of it gets reflected as shown in Fig. 5.10. However, at $\theta = 60^0$, as the $\vec{J} \times \vec{B}$ force is relatively weaker the penetration in plasma is much less and the laser pulse as a whole almost gets reflected and propagates almost parallel to the surface through vacuum. Thus, the current density is found to be more at $\theta = 30^0$. Fig. 5.11 depicts the saturation of magnetic energy with time. The magnetic energy increases very sharply up to $\approx$ 75.40 T_0 and then gets saturated. However, the magnetic energy decreases with an increase in angle of incidence. The formation of strong current

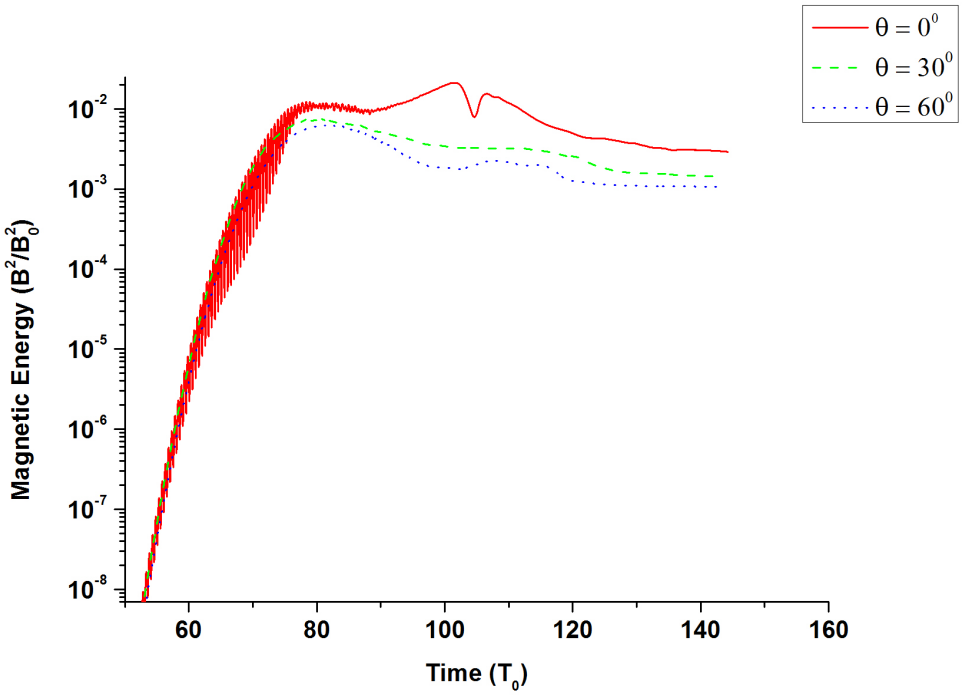

Fig. 5.11: Normalized magnetic energy (B^2/B_0^2) vs Time (T_0) for $\theta = 0^0$ (red solid), $\theta = 30^0$ (green dashed) and $\theta = 60^0$ (blue dotted).

carrying filaments decreases as the angle of incidence is increased. Since, a strong current carrying filament is formed when the laser is incident normally ($\theta = 0^0$) on the plasma slab, the magnetic energy is highest in case of normal incidence.

5.4 Conclusion

The role played by the angle of incidence of a short pulse linearly polarized laser in the formation of periodic magnetic field structures in overdense plasmas has been investigated with the help of 3D-PIC simulations. The simulations have been done for different angles of incidence $\theta = 0^0$, 30^0 and 60^0. The conclusions drawn from the above discussions can be summarized as follows :

i) Huge magnetic fields of the order of $\approx$ 400 MG are generated when the laser is incident normally on the target. The laser pulse gets focussed up to a very short length of 2 μm inside the target and the axial intensity rises up to a maximum of $\approx$ 11 times the fundamental laser intensity.

ii) At $\theta = 30^0$, the laser pulse penetrates up to some distance inside the plasma and a part of it gets reflected whereas at $\theta = 60^0$, the penetration in plasma is

much less and the laser pulse as a whole gets reflected and propagates almost parallel to the surface through vacuum.

iii) Periodic density ripple like structures are formed due to emission of energetic electron jets from the plasma surface which may be due to vacuum heating. These ripples carry forward and return currents which re responsible for the formation of periodic magnetic field structures on the plasma surface.

iv) The formation of density ripples are found to be more prominent at $\theta = 60^0$ due to efficient vacuum heating and the inter spacing distance coincides with the laser wavelength ($\lambda = 1$ μm).

Bibliography

[1] Wilks, S. C., Kruer, W. L., Tabak, M., and Langdon, A. B. Absorption of ultra-intense laser pulses. *Phys. Rev. Lett.*, 69:1383–1386, 1992.

[2] Sandhu, A. S., Dharmadhikari, A. K., Rajeev, P. P., Kumar, G. R., Sengupta, S., Das, A., and Kaw, P. K. Laser-generated ultrashort multimegagauss magnetic pulses in plasmas. *Phys. Rev. Lett.*, 89:225002, 2002.

[3] Mondal, S., Narayanan, V., Ding, W. J., Lad, A. D., Hao, B., Ahmad, S., Wang, W. M., Sheng, Z. M., Sengupta, S., Kaw, P., Das, A., and Kumar, G. R. Direct observation of turbulent magnetic fields in hot, dense laser produced plasmas. *Proceedings of the National Academy of Sciences*, 109(21):8011–8015, 2012.

[4] Weibel, E. S. Spontaneously growing transverse waves in a plasma due to an anisotropic velocity distribution. *Phys. Rev. Lett.*, 2:83–84, 1959.

[5] Stamper, J. A., Papadopoulos, K., Sudan, R. N., Dean, S. O., McLean, E. A., and Dawson, J. M. Spontaneous magnetic fields in laser-produced plasmas. *Phys. Rev. Lett.*, 26:1012–1015, 1971.

[6] Haines, M. G. Saturation mechanisms for the generated magnetic field in nonuniform laser-matter irradiation. *Phys. Rev. Lett.*, 78:254–257, 1997.

[7] Sudan, R. N. Mechanism for the generation of 10^9 g magnetic fields in the interaction of ultraintense short laser pulse with an overdense plasma target. *Phys. Rev. Lett.*, 70:3075–3078, 1993.

[8] Pukhov, A. and Meyer-ter Vehn, J. Laser hole boring into overdense plasma and relativistic electron currents for fast ignition of icf targets. *Phys. Rev. Lett.*, 79: 2686–2689, 1997.

[9] Lasinski, B. F., Langdon, A. B., Hatchett, S. P., Key, M. H., and Tabak, M. Particle-in-cell simulations of ultra intense laser pulses propagating through overdense plasma for fast-ignitor and radiography applications. *Physics of Plasmas*, 6(5):2041–2047, 1999.

[10] Okada, T., Ogawa, K., and Sugie, M. Three-dimensional particle-in-cell simulations of energetic electron generation and self-generated magnetic field with high-intensity laser pulses in overdense plasmas. *Journal of Plasma Physics*, 72 (6):925928, 2006.

[11] Sentoku, Y., Mima, K., Sheng, Z. M., Kaw, P., Nishihara, K., and Nishikawa, K. Three-dimensional particle-in-cell simulations of energetic electron generation and transport with relativistic laser pulses in overdense plasmas. *Phys. Rev. E*, 65:046408, 2002.

[12] Catto, P. J. and More, R. M. Sheath inverse bremsstrahlung in laser produced plasmas. *The Physics of Fluids*, 20(4):704–705, 1977.

[13] Kruer, W. L. and Estabrook, K. Jb heating by very intense laser light. *The Physics of Fluids*, 28(1):430–432, 1985.

[14] Brunel, F. Not-so-resonant, resonant absorption. *Phys. Rev. Lett.*, 59:52–55, 1987.

[15] Gamaliy, E. G. and Dragila, R. Interaction of ultrashort laser pulses at relativistic intensities with solid targets: Relativistic skin effect. *Phys. Rev. A*, 42: 929–935, 1990.

[16] Tatarakis, M., Gopal, A., Watts, I., Beg, F. N., Dangor, A. E., Krushelnick, K., Wagner, U., Norreys, P. A., Clark, E. L., Zepf, M., and Evans, R. G. Measurements of ultrastrong magnetic fields during relativistic laserplasma interactions. *Physics of Plasmas*, 9(5):2244–2250, 2002.

[17] Sentoku, Y., Ruhl, H., Mima, K., Kodama, R., Tanaka, K. A., and Kishimoto, Y. Plasma jet formation and magnetic-field generation in the intense laser plasma under oblique incidence. *Physics of Plasmas*, 6(7):2855–2861, 1999.

[18] Okada, T. and Ogawa, K. Saturated magnetic fields of weibel instabilities in ultraintense laser-plasma interactions. *Physics of Plasmas*, 14(7):072702, 2007.

[19] Upadhyay, A., Patel, K., Rao, B. S., Naik, P. A., and Gupta, P. D. Three-dimensional simulation of laser–plasma-based electron acceleration. *Pramana*, 78(4):613–623, 2012.

[20] Akhiezer, A. and Polovin, R. Theory of wave motion of an electron plasma. *Soviet Phys. JETP*, Vol: 3, 1956.

[21] Kaw, P. and Dawson, J. Relativistic nonlinear propagation of laser beams in cold overdense plasmas. *The Physics of Fluids*, 13(2):472–481, 1970.

[22] Max, C. and Perkins, F. Strong electromagnetic waves in overdense plasmas. *Phys. Rev. Lett.*, 27:1342–1345, 1971.

[23] Naumova, N. M., Bulanov, S. V., Nishihara, K., Esirkepov, T. Z., and Pegoraro, F. Polarization effects and anisotropy in three-dimensional relativistic self-focusing. *Phys. Rev. E*, 65:045402, 2002.